Processing of All-Oxide Ceramic Matrix Composites with RBAO Matrices

P.O. Guglielmi[*1], D.E. García[2], M.P. Hablitzel[2], D. Blaese[1], D.P. Goulart[2], A. Borchert[1], D. Hotza[3], R. Janssen[1]

[1]Institute of Advanced Ceramics, Hamburg University of Technology (TUHH), Denickestrasse 15, 21073 Hamburg, Germany
[2]Department of Mechanical Engineering (EMC), Federal University of Santa Catarina (UFSC), 88040 – 970 Florianópolis, Brazil
[3]Department of Chemical Engineering (EQA), Federal University of Santa Catarina (UFSC), 88040 – 970 Florianópolis, Brazil

Abstract

A methodology to produce full-scale, all-oxide composites with porous reaction-bonded aluminum oxide (RBAO) matrices is presented. Composites are produced by a two-step impregnation route, in which alumina fiber fabrics are first infiltrated with an ethanol-based slurry of the RBAO particles and then laminated between layers of an RBAO-loaded paraffin-based suspension to produce thermoplastic prepregs. The composition of the RBAO precursor powders is tailored for each of these suspensions, so that low-to-zero shrinkage is achieved during sintering and all-oxide composites with a reduced amount of shrinkage-related matrix cracks are produced. Processing challenges faced during the development of these composites are presented and discussed. These include the formation of matrix voids owing to the evaporation of volatile species from the RBAO powder surfaces that remain entrapped in the paraffin-based suspension during lamination. Despite these voids, composites containing ~ 36 vol% fibers exhibit a flexural strength of ~ 240 MPa, together with a non-catastrophic, stepwise failure, similar to that of layered ceramics.

Keywords: Ceramic matrix composites, RBAO, processing, microstructure, properties

I. Introduction

The mitigation of shrinkage-related matrix cracks formed during composite processing is a current challenge in the development of ceramic matrix composites (CMCs). These cracks form predominantly in CMCs reinforced with two-directional (2D), long-fiber woven fabrics owing to the constrained shrinkage imposed by the rigid network of fibers during drying and sintering of the matrix [1–3]. Avoiding the formation of these cracks is essential for enhancing the mechanical properties of the material [4–6], as well as its thermal conductivity, which leads to a higher thermal shock resistance [7,8].

In order to produce crack-free CMCs, the shrinkage of the matrix during processing must be reduced to zero. Reaction-bonded aluminum oxide (RBAO) emerges then as a promising matrix material to produce crack-free all-oxide composites. RBAO precursor powders contain metallic aluminum particles that oxidize during heat treatment in air to form alumina. By tailoring the aluminum content of the precursor powder, the expansion associated with this oxidation can partially or totally compensate for the shrinkage of the RBAO ceramics at a given sintering temperature, so that ceramic parts with low-to-zero shrinkage

can be produced [9,10]. Nevertheless, although often suggested in the literature [2,11,12], there is to date no report of the use of RBAO in the production of full-scale, all-oxide composites. Research in this area has been restricted to the analysis of model and mini composites consisting of a few fibers or tows dispersed in the matrix [11–13]. Therefore, the possible benefits and drawbacks of using RBAO to produce all-oxide CMCs and the related effects on the final material properties are still unclear.

This work aims at investigating the viability of using RBAO to produce all-oxide CMCs with a reduced amount of shrinkage-related cracks. Owing to the high reactivity of aluminum particles with water [10], conventional CMC processing routes based on the infiltration of fiber fabrics with aqueous slurries cannot be used. Instead, a recently developed manufacturing route [14,15] completely based on organic particle carriers is used in this work. In this route, a paraffin-based suspension of the matrix particles is used to laminate 2D thermoplastic prepregs that are stable and easy to handle at room temperature and that can be joined and shaped at temperatures above the softening point of the binder system. Nevertheless, paraffin-based suspensions are too viscous to percolate through the fiber bundles of the woven fabrics. Therefore, a low-viscous ethanol-based slurry is used to infiltrate matrix particles

* Corresponding author: paula.guglielmi@hzg.de

within the fiber bundles prior to the prepreg lamination procedure. This results in a two-step impregnation route, in which the intra-bundle spaces are filled with matrix particles by the low-viscous ethanol-based slurry and the large inter-bundle spaces located at the crossover between fiber bundles are filled with the paraffin-based suspension during the lamination of thermoplastic prepregs [14, 15]. This two-step impregnation route allows for a homogenous distribution of matrix particles throughout the green composites, so that shrinkage and cracks are avoided also in the green state [14, 15].

Based on this novel prepreg lamination route, a methodology is proposed here to produce full-scale, 2D all-oxide composites with low-to-zero shrinkage RBAO matrices. Processing challenges faced during the development of these composites are presented and discussed. Processing is evaluated in terms of the resulting microstructure and flexural behavior of the different RBAO-matrix composites produced.

II. Experimental Procedure

(1) RBAO powder processing and characterization

Several RBAO powder compositions with varying aluminum contents of 10, 20, 26, 30, 40 and 50 vol% were prepared by means of attrition milling (Netzsch PE 075, Netzsch Feinmahltechnik, Germany) in acetone, at 700 rpm for 7 h. In all RBAO compositions, aluminum powder (ECKA AS 081, 20 μm average particle size, Eckart-Werke, Wackersdorf, Germany) was milled together with 10 vol% coarse alumina powder (Almatis T60, 13 μm average particle size, USA), 20 vol% fine yttria-stabilized zirconia (YSZ) powder (TZ-3Y, 28 nm average crystallite size, Tosoh, Toyama, Japan) and a fine alumina powder (Ceralox HPA 0.5, 0.4 μm average particle size, RWE-DEA, Hamburg, Germany). The amount of fine alumina was adjusted depending on the amount of aluminum used, to complete 100 % in the compositions. The different powder mixtures are designated here RB10, RB20, RB26, etc., with the two digits indicating the amount of aluminum used. The coarse alumina particles were added to enhance the milling efficiency and achieve a final aluminum particle size of ~ 1 μm, which is important for a successful oxidation process [16]. YSZ was added to the RBAO powder mixtures since it enhances the oxidation kinetics of the aluminum particles [17, 18] and hinders the grain growth of alumina, leading to fine-grained, homogeneous microstructures and improved mechanical properties [10]. Attrition milling was performed on 100-g powder batches, in a 500-cm³ alumina crucible, using 1500 g of 3-mm zirconia balls (YTZ grinding media, Tosoh, Toyama, Japan). After milling, the RBAO powders were dried for 48 h at room temperature in a drying cupboard, and subsequently sieved (200-μm opening sieve) in a vibratory sieve shaker (AS 200 digit, Retsch, Germany) for deagglomeration. Hereafter, these powders will be referred to as as-milled powders. In some cases, these powders were subsequently dried in a muffle furnace at 300 °C for 10 h, to thermally remove chemical species adsorbed on the powder surfaces during milling. The use of such dried powders will be explicitly indicated in the text.

The particle size distributions of powders RB26 and RB30 were measured by means of laser diffraction using a Mastersizer S (Malvern Instruments, Herrenberg, Germany). For that, a sample of the milling slurry (~ 1 ml) was collected after 7 h milling using a pipette and dispersed in ~ 4 ml ethanol. Before measuring, the slurry was sonicated for the purpose of deagglomeration.

To evaluate the mass change and the presence of reactions as a function of temperature, thermogravimetry (TG) was performed together with differential thermal analysis (DTA) on as-milled RB20 and RB30 powders. This was conducted in a simultaneous thermal analyzer (STA 409, Netzsch, Selb, Germany), from room temperature to 650 °C at 1 °C/min.

Karl-Fischer titration (Aqua 40.00, Electrochemie GmbH, Halle, Germany) was used to measure the water content present on the surface of the as-milled RB30 powder. A total of four measurements was made on different samples of the same powder. Samples were heated to 150 °C during the measurements.

(2) Determination of zero-shrinkage compositions

The use of two different suspensions in the composite processing route used in this work leads to the formation of two slightly different oxide matrices after sintering: an *intra-bundle matrix* (IB), originated from the ethanol-based slurry, and an *inter-textile matrix* (IT), originated from the paraffin-based suspension [14, 15]. These matrices may present different sintering shrinkages owing to different starting green densities. Therefore, the amount of aluminum necessary for shrinkage compensation must be tailored for each suspension separately. The next sections present how the compositional tailoring was performed for RBAO composite matrices to be sintered at 1200 °C for 30 min, following the heating cycle schematically shown in Fig. 1. This temperature was selected in order to avoid excessive grain growth of the polycrystalline alumina fibers used (Nextel™ 610) [2, 19].
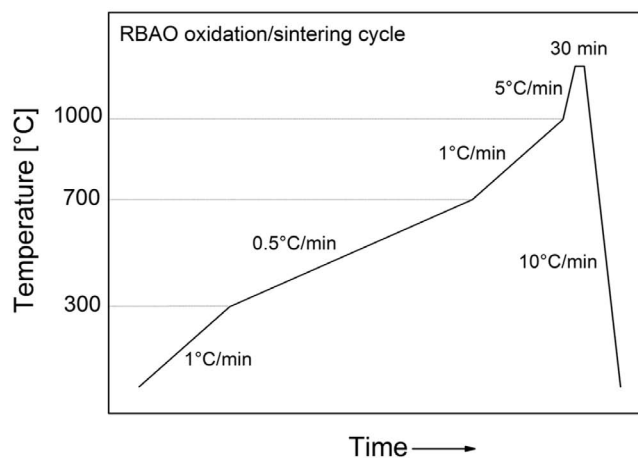

Fig. 1: Heating cycle used to sinter the RBAO-matrix composites analyzed in this work.

(a) RBAO composition for the intra-bundle (IB) matrix

In order to estimate the amount of aluminum necessary for compensating the shrinkage of the IB matrix, the linear dimensional change (LDC) of RBAO samples contain-

ing different amounts of aluminum was investigated by means of dilatometry. Green RBAO matrix samples were prepared by means of uniaxial pressing (WCH 10, P/O/Weber, Remshalden, Germany) of as-milled RBAO powders containing 10, 20 and 30 vol % aluminum at 15 MPa for 30 s, followed by cold isostatic pressing (KIPP 200ES, P/O/Weber) at 300 MPa for 2 min. Samples were ground to the dimensions of 12 mm × 4 mm × 4 mm and heated to 1200 °C in a dilatometer (DIL 402 PC, Netzsch, Selb, Germany), following the heating rates shown in Fig. 1. The samples were held at this temperature for 5 h. Based on the dilatometry results, it was possible to calculate the linear dimensional change of each RBAO matrix composition (LDC_{IB}) after sintering at 1200 °C for 30 min. The obtained values of LDC_{IB} were fitted to a linear function of the form

$$LDC_{IB} = LDC_0(\kappa v_{Al} - 1) \qquad (1)$$

where v_{Al} is the volume fraction of aluminum, LDC is the linear dimensional change for $v_{Al}=0$ and κ is a constant. This equation was then used to calculate the aluminum amount necessary for achieving zero shrinkage in the IB matrix.

(b) *RBAO composition for the inter-textile (IT) matrix*

To achieve low-to-zero shrinkage in the IT matrix, the aluminum amount in the RBAO powder should not only compensate for the shrinkage owing to sintering, but also for the shrinkage owing to pyrolysis of the organic binder system. In order to determine the most appropriate combination of aluminum amount in the RBAO powder and the solid content of the paraffin-based suspension, a total of six suspensions was produced using either the as-milled RB20 or the RB30 powder and solid contents of 50, 54 and 58 vol%. Table 1 shows the composition of paraffin-based suspensions with the different solid contents investigated in this work. Details on the composition of the binder system and on the preparation of the paraffin-based suspensions can be found elsewhere [14, 15]. Briefly, all organic components were pre-heated at 100 °C and mixed in a glass beaker. The RBAO powder was then slowly added and mixed with a glass stirrer. Further homogenization was obtained by passing the suspensions several times through a three-roller mill (EXAKT 120S, EXAKT, Norderstedt, Germany) heated at 95 °C. After homoge-

nization, the suspensions were molded to discs by softening them at 115 °C into cylindrical aluminum forms with a diameter of ~ 38 mm. Debinding was performed thermally, according to previous works reported on the binder system used [14, 20, 21]. Sintering was conducted at 1200 °C for 30 min, following the thermal cycle shown in Fig. 1. The linear dimensional change of the disc-shaped IT matrix samples (LDC_{IT}) was determined by comparing the diameter of the samples measured before and after the debinding/sintering procedure.

(3) *Composite processing*

The RBAO powder compositions selected for the IB and IT matrices will be presented in Section III (1), together with the solid content selected for the paraffin-based suspension. The selected RBAO matrix powders were employed in this work in two drying conditions to manufacture two different composites, as follows:
(i) as-milled powders, dried at room temperature for 48 h (composite $RB_{(RT)}$CMC);
(ii) powders dried at 300 °C for 5 h in a muffle furnace (composite $RB_{(300)}$CMC).

The processing steps used in this work to manufacture RBAO-matrix composites are described in the following subsections. More details on this processing route can be found elsewhere [14, 15].

(a) *Fibers*

Commercial 2D alumina fiber fabrics (Nextel™ 610, 8 harness satin, 1500 denier, 3M, Neuss, Germany) were used as reinforcement. The fiber textile was cut into 110 mm × 100 mm pieces and desized at 700 °C for 30 min in a muffle furnace.

(b) *Preparation of suspensions*

Ethanol-based slurries containing 32 vol% solids were prepared in an attrition mill by mixing the selected RBAO powder in ethanol, using 0.6 wt% Dolacol D 1001 (Zschimmer & Schwarz, Lahnstein, Germany) as a deflocculant. The slurry was mixed for 15 min at 500 rpm in a 500-cm³ alumina crucible containing 1300 g of 3 mm zirconia balls. After mixing, the RBAO slurry was poured into a glass beaker for the subsequent infiltration of fiber textiles.

Table 1: Composition of the paraffin-based suspensions analyzed in this work.

Material	Producer	Density (g/cm³)	Volume Content of Solids		
			58 vol%	56 vol%	54 vol%
RBAO powder	(this work)	Various[a]	58	56	54
Paraffin KX1313	Zschimmer & Schwarz	0.9	35.44	37.13	38.82
Octadecylamine	Sigma-Aldrich	0.9	2.96	3.10	3.24
Licowax OP	Clariant	1.0	2.52	2.64	2.76
Solsperse	Zencca	0.9	1.08	1.13	1.18

a) True densities of the as-milled RB20 and RB30 powders were 3.88 g/cm³; and 3.69 g/cm³;, respectively, as determined by means of He-pycnometry.

Paraffin-based suspensions were prepared according to the procedure described in Section III(2). After homogenization on the three-roller mill, the suspensions were allowed to solidify at room temperature and then granulated with a mortar and pestle to facilitate their handling through the consecutive processing steps.

(c) *Composite lamination, debinding and sintering*

To produce prepregs, the desized fiber textiles were immersed into the ethanol-based slurry for the impregnation of the fiber bundles. After 20 min, the textiles were removed from the suspension and allowed to dry in air for 2 h. Thermoplastic prepregs were manufactured by manually laminating the pre-infiltrated fiber textile between layers of the softened, granulated paraffin-based suspension onto a heating plate at 115 °C. Aluminum foils were used during this lamination procedure to prevent the molten suspension from adhering to the heating plate or to the laminating roll. The prepregs were then joined by means of manual lamination to consolidate green composites. While eight prepreg layers were joined in a cross-ply configuration in composite $RB_{(RT)}CMC$, only six prepregs were joined for composite $RB_{(300)}CMC$, owing to the larger thickness of the prepregs produced with RBAO powders dried at 300 °C. The green CMC bodies were subsequently shaped by means of warm pressing (~0.5 MPa) between two flat metal plates heated to 115 °C, to obtain plan-parallel composite plates for the mechanical characterization. Debinding was performed thermally, according to a procedure described elsewhere [14,20,21]. Sintering was performed in air, in a box furnace at 1200 °C for 30 min.

(4) *Composite characterization*

Microstructural analysis was conducted by means of SEM (ZEISS Supra VP 55, Carl Zeiss, Oberkochen, Germany) on polished cross-sections of the RBAO-matrix composites.

Composite density was measured geometrically on specimens used for mechanical testing. Fiber volume fraction v_f of the sintered composites was also calculated geometrically, according to:

$$v_f = \frac{nm_{tex}}{h\rho_f} \qquad (2)$$

where n is the total number of textile layers used in the composite, m_{tex} is the mass per unit area of textile, h is the composite thickness, and r_f is the fiber density (3.9 g/cm³, as provided by the supplier). A value of m_{tex} 0.0359 g/cm² was measured for the desized Nextel™ 610 woven fabric used in this work.

Four-point bending tests (4PB) were conducted according to the German standard DIN EN 658 – 3 [22]. All tests were performed at room temperature, on 0°/90°-oriented test specimens. Load was applied in a direction perpendicular to the laminate plane. Bending bars were cut from the sintered composite plates using a diamond cutting disc. The specimens were 90 mm long and 10 mm wide. The thickness of the 4PB specimens was determined by the thickness of the composites after sintering. A thickness of 2.06 ± 0.07 mm was obtained for composite $RB_{(RT)}CMC$,

while a value of 2.65 ± 0.04 mm was measured for the $RB_{(300)}CMC$ composite. As will be discussed in Section 2.9, the difference in the thickness of these composites is associated with the thicker IT matrix layers of composite $RB_{(300)}CMC$ when compared to composite $RB_{(RT)}CMC$.

The specimens were tested in a universal testing machine (Zwick 1474, 100 kN, Zwick, Ulm, Germany) with load and support spans of 25 mm and 75 mm, respectively. A thin polymer film was placed between the samples and the loading rollers in order to minimize friction stresses during testing. Deflection was measured with an inductive displacement transducer placed at the tensile side of the specimens, at the middle of the load span. Samples were loaded at 1 mm/min. At least eight samples of each RBAO-matrix composite were tested. Nominal flexural stresses σ and outer fiber strains ε were determined on the basis of elastic bending, according to [22,23]:

$$\sigma = \frac{3L(S - S_i)}{2bh^2} \qquad (3)$$

$$\varepsilon = 4.70\frac{dh}{S^2} \qquad (4)$$

where L is the load acting on the sample, b is the sample width, h is the composite sample thickness, d is the deflection of the specimen at the middle of the load span and S_i and S are the inner and outer loading spans, respectively. The composite flexural modulus E_c was calculated for each specimen as the slope of the stress-strain curve within the initial linear-elastic region.

Fracture surfaces of representative 4PB specimens were observed with a 3D Infinite Focus microscope (Alicona, Raaba, Austria-Graz).

III. Results and Discussion

(1) *Determination of zero-shrinkage composition*

The results of the dilatometric analyses performed on as-milled RBAO powders containing 10, 20 and 30 vol% aluminum are shown in Fig. 2. The higher the aluminum content, the larger the expansion owing to the oxidation of aluminum particles and the smaller the resulting shrinkage after cooling. The major expansion occurs up to 600 °C. Beyond this temperature, the LDC remains nearly constant, until the melting temperature of aluminum ($T_{Al} = 660 °C$) is achieved, leading to a slight contraction of the sample. Oxidation proceeds then by liquid/gas reaction, without significant further dimensional change. At ~ 1050 °C, all samples start to shrink owing to sintering.

The values of LDC_{IB} calculated after sintering at 1200 °C for 30 min are presented in Fig. 3. The experimental data was fitted with Eq. 1, with LDC_0 1.78 and κ 3.8. Using this equation, the aluminum content necessary to achieve zero shrinkage in the IB matrix was calculated as ~ 26 vol%. This RBAO powder, designated here RB26, was then used in the preparation of the ethanol-based slurry described in Section II(3)(b).
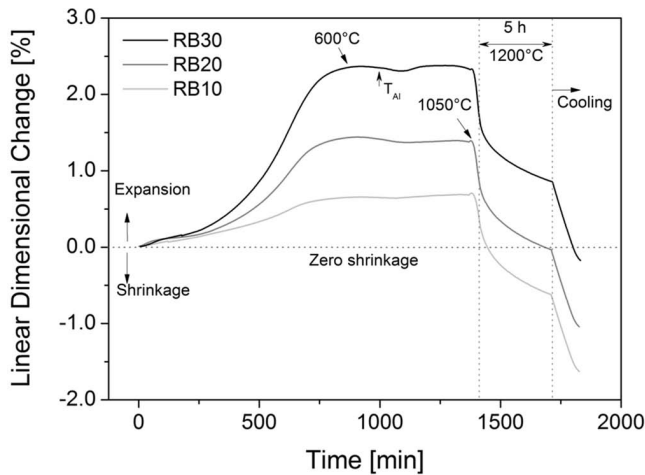
Fig. 2: Dilatometry curves of cold-isostatic-pressed RBAO samples containing different amounts of aluminum. T_{Al} indicates the melting temperature of aluminum.
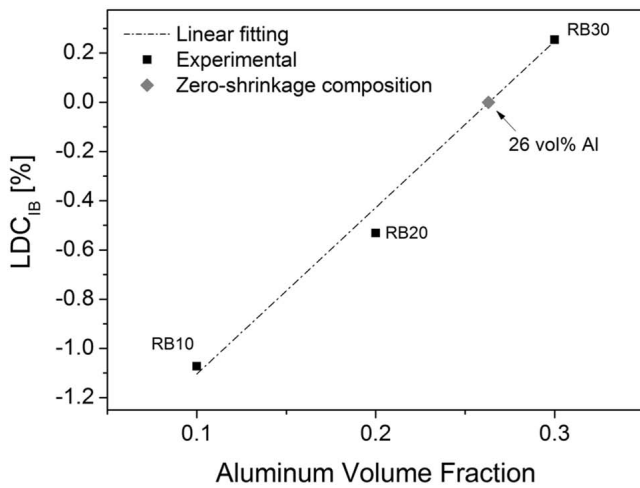

Fig. 3: Linear dimensional change calculated from dilatometry data for cold-isostatic-pressed RBAO samples containing different amounts of aluminum, considering a 30-min sintering at 1200 °C.

Fig. 4 shows the linear dimensional change of RBAO matrix samples produced with paraffin-based suspensions as a function of aluminum amount and solid content. The shrinkage of the monolithic IT matrix samples decreased with increasing the solid content of the paraffin-based suspensions. Additionally, samples produced with powders containing 30 vol% aluminum presented lower shrinkages than those produced with powders containing 20 vol% aluminum. The sample that most approaches zero shrinkage is the one produced with an RB30-loaded suspension containing 58 vol% solids. However, the rheology of this suspension was not adequate for the manufacture of prepregs. Poor adhesion between this paraffin-based suspension and the pre-infiltrated fiber textiles, as well as the impossibility of obtaining thin prepregs, are some of the problems observed. Reducing the solid content to 56 vol% enabled successful prepreg manufacture by means of lamination. Therefore, as indicated in Fig. 4, the composition containing 30 vol% aluminum and 56 vol% solids was selected to be used in the IT matrix of the CMCs. Although the shrinkage associated with this composition is not zero,

it is very low (~ 1 %) and should suffice to reduce the formation of shrinkage-related cracks in the RBAO-matrix composites.
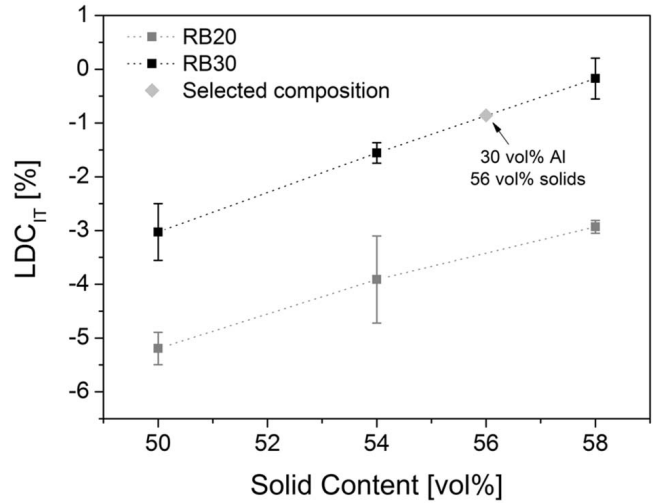

Fig. 4: Linear dimensional change of RBAO samples produced with paraffin-based suspensions with different solid contents. The suspensions were prepared with powders containing 20 and 30 vol% aluminum. The dotted lines were drawn to help guide the eye.

The particle size distributions of the low-to-zero RBAO powder compositions selected for the composite manufacture are presented in Fig. 5. Both RB26 and RB30 powders exhibit a narrow particle size distribution with a median size, D50, of ~ 1.3 µm, which is in the range recommended for a successful oxidation process. The monomodal particle size distributions indicate that particle agglomeration takes place during milling, since it is not possible to differentiate between the aluminum particles and the very small oxide particles used in the powder mixtures (fine-grained alumina and YSZ).
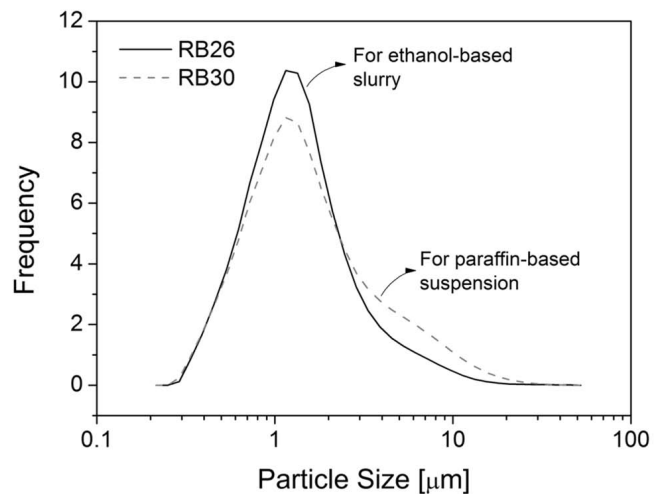

Fig. 5: Particle size distributions after 7 h milling of the RBAO powder compositions selected to be used in the processing of RBAO-matrix, all-oxide composites.

(2) Microstructure and processing challenges

The microstructure of the $RB_{(RT)}CMC$ composite is presented in Fig. 6. The intra-bundle and inter-textile matrices are indicated in the pictures by IB and IT, respectively. A fiber volume content of 36 vol% was obtained in this

composite. Tailoring the RBAO matrix composition was effective to achieve low-to-zero shrinkage and fabricate a composite without the shrinkage-related cracks typical for all-oxide composites reinforced with 2D fiber textiles. Nevertheless, the formation of large voids in the IT matrix regions was observed. These voids vary from tens to hundreds of micrometers in size, some being spherical and others elongated in the lamination direction. Using image analysis of six different micrographs at magnifications between 75× and 300×, a void volume fraction of 6 ± 3 vol% was determined for the RB$_{(RT)}$CMC. The large scatter of this data is due to the irregular distribution of voids in the samples. Since such voids can be detrimental to the mechanical properties of the composite [24–27], the potential causes for their formation are investigated and a possible solution is proposed here for their mitigation.
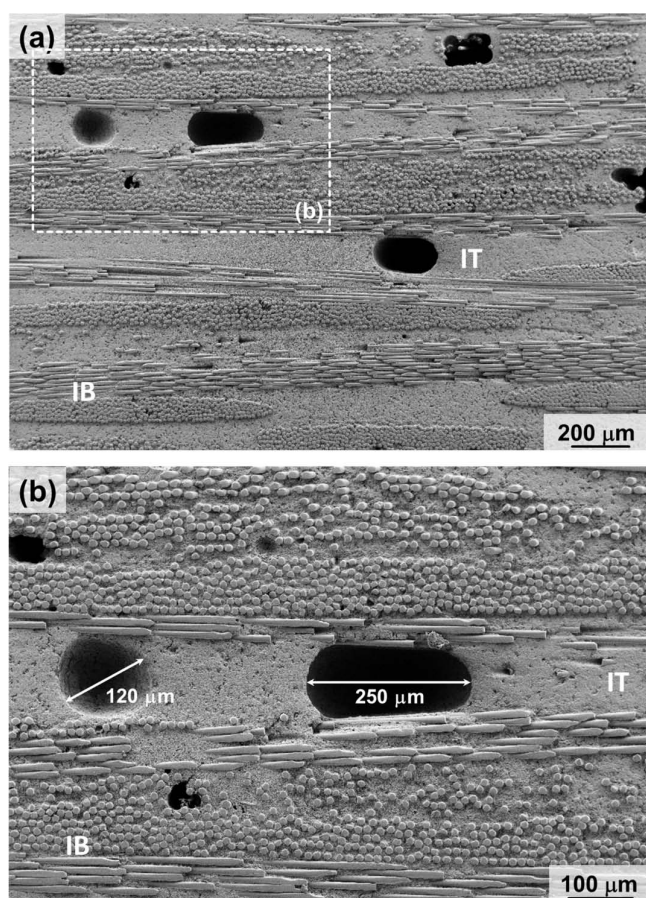

Fig. 6: Microstructure of composite RB$_{(RT)}$CMC, produced with RBAO powders dried at room temperature for 48 h (as-milled condition). Sintering was performed at 1200 °C for 30 min. (b) shows a higher magnification image of the region indicated in (a).

According to experimental observations, these voids originate from entrapped gas bubbles that evolve in the paraffin-based suspension as soon as the suspension is softened at a temperature of ~115 °C. A possible cause for the formation of these bubbles is the evaporation of adsorbed species from the powder surfaces. RBAO powders used in this work are prepared by intensively milling in acetone for 7 h. The high solubility of water in acetone leads to the absorption of moisture from the atmosphere during milling and, as a consequence, newly-formed aluminum surfaces readily react with water to form oxides and hydroxides [10]. Although the passivation of aluminum

particles is advantageous in terms of the safe handling of the RBAO precursor powders, it has been reported that the evaporation and decomposition of chemical species from the particle surfaces during processing may lead to defects in the final ceramics, such as bloating and voids originating from entrapped gases [10, 28]. In the case of RBAO samples manufactured by dry processing routes at room temperature, such as uniaxial and cold isostatic pressing, such defects can be inhibited by using slow heating rates in the sintering cycle, so that the volatile species have time to escape through the open pores of the sample before densification. However, in a wet processing route where a viscous media such as molten paraffin is used, and temperature is required for the conformation procedure, desorption of molecules can lead to entrapped gas bubbles in the material.

The amount of adsorbed water on the as-milled RBAO powder was determined in this work by means of Karl-Fischer titration. Results indicate the presence of 4.8 ± 0.7 wt% water on the surface of the RB30 powder, which is in good agreement with measurements conducted by Temuujin *et al.* [29] for an RBAO powder containing 30 vol% aluminum and dried in air at room temperature. This result indicates that the large voids present in the IT matrix of the composite RB$_{(RT)}$CMC can be originated from water desorption from the RB30 powder surfaces during the lamination procedure conducted at ~115 °C.

To evaluate this hypothesis, RB30 powders were dried for 10 h in a muffle furnace at temperatures of 100, 200 and 300 °C and used to conform disc-shaped RBAO matrix samples according to the procedure described in Section II(2)(b), using 56-vol%-loaded, paraffin-based suspensions. Cross-sections of these monolithic matrix samples were analyzed after sintering and are presented in Fig. 7, together with a sample prepared with an RB30 powder in the as-milled condition.

The sample produced with the as-milled powder (Fig. 7 (a)) presents the largest amount of voids, whose sizes vary from ~100 to ~1000 μm. Drying the powder at 100 °C for 10 h (Fig. 7 (b)) reduces the amount of voids, although they are still large. Drying temperatures of 200 °C or 300 °C (Fig. 7 (c) and (d), respectively) are more effective in reducing the formation of voids, although they are not completely eliminated. Holz *et al.* [10] showed that physically adsorbed water on RBAO powder surfaces is completely eliminated up to ~250 °C. Therefore, if bubble formation was exclusively a result of the desorption of physically bound water from the RBAO powder surfaces, no voids should be observed in the sample produced with the powder dried at 300 °C for 10 h. Since it is not the case, there must be another factor contributing to the bubble formation in the RBAO-loaded paraffin-based suspensions.

Fig. 8 shows the results of the simultaneous thermal analysis performed on the as-milled RB20 and RB30 powders. The mass loss endured by RBAO powders up to 300 °C has been often associated with the desorption of physically bound water and molecules from the milling liquid, as well as to the decomposition of aluminum hydroxides [10, 30, 31]. The exothermic peak at ~507 °C has been often related

to the solid/gas oxidation of aluminum particles [10]. To the best of our knowledge, however, no previous work has explained the origin of the broad exothermic peak between ~ 112 °C and ~ 315 °C so far. Similar to the oxidation peak at ~ 507 °C, the intensity of this broad peak is influenced by the aluminum amount present in the powder. The higher the aluminum content, the more intense is the peak.
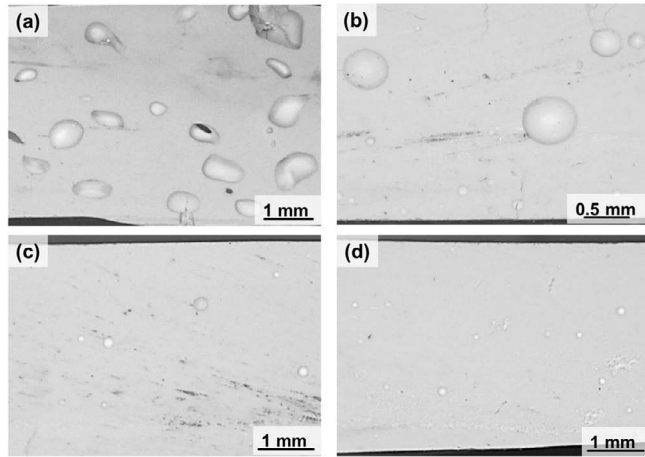

Fig. 7: Monolithic IT matrix samples prepared with paraffin-based suspensions containing RB30 powders in different conditions: (a) dried at room temperature for 48 h, (b) dried at 100 °C for 10 h, (c) dried at 200 °C for 10 h and (d) dried at 300 °C for 10 h. All suspensions contained 56 vol% solids. After debinding, sintering was performed at 1200 °C for 30 min.
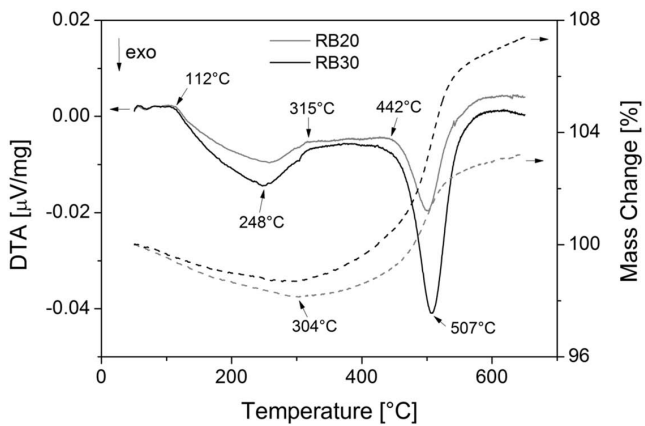

Fig. 8: Simultaneous thermal analysis of RBAO powders containing 20 vol% and 30 vol% aluminum..

Although desorption and hydroxide decomposition contribute to the mass loss up to 300 °C, both reactions are endothermic processes [32, 33], and it is suggested here that the exothermic peak between ~ 112 °C and ~ 315 °C is originated from a reaction between the aluminum particles of the RBAO powder and the water evaporated from the powder surfaces, which releases H_2 as a by-product, for instance, according to [34]:

$$Al + 2H_2O \rightarrow AlOOH + 3/2H_2 \uparrow \qquad (5)$$
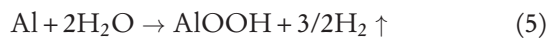
Supporting this idea are the results of mass spectroscopy conducted by Holz *et al.* [10], which show that H_2 molecules start being released at ~ 80 °C, accompanying the desorption of water. Reactions of aluminum and water-liberating H_2 are used for different technical

purposes, such as pore formation in the fabrication of cellular concrete [35, 36] and hydrogen production for energy generation (via fuel cells) [34, 37–39]. Different investigations [37, 38] on materials for fuel cell applications showed that aluminum powder may react completely with water, even at room temperature. For this purpose, aluminum must be intensively milled with aluminum oxide or hydroxide powders [37, 38] and, in some cases, have its surface modified by a reaction with $Al(OH)_3$ to form a loose γ-alumina layer on the aluminum particles [38]. An explanation for the effect of oxides on the enhanced reactivity of aluminum with water was suggested by Deng *et al.* [34]. It was postulated that the alumina layer present on the aluminum particle surfaces may completely hydrate when in contact with water to form boehmite (AlOOH) [34]:

$$Al_2O_3 + H_2O \rightarrow 2AlOOH \qquad (6)$$

The OH^- ions, which are suggested to be the mobile species in these hydrated films [40], can then diffuse to the aluminum-boehmite interface and react with the metallic aluminum to form alumina and H_2 molecules [34]:

$$6AlOOH + 2Al \rightarrow 4Al_2O_3 + 3H_2 \qquad (7)$$
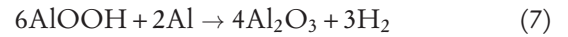
Since the H_2 molecules do not easily diffuse through the alumina film, they accumulate and form gas bubbles in the aluminum-alumina interface [34]. Under favorable conditions of temperature and pressure, these bubbles can rupture the hydrated oxide film on the particle surface and expose the metallic aluminum to the surrounding water. This leads to the formation of boehmite, again liberating H_2, according to Eq. 5.

There are clear similarities between RBAO powder mixtures and these modified aluminum powders used for H_2 generation: (a) RBAO powder is also prepared by intensively milling aluminum and oxide particles; (b) it has been shown that the surfaces of aluminum particles in RBAO are modified during milling by the formation of amorphous alumina and aluminum hydroxides (boehmite and diaspore) [10, 41]; (c) RBAO powders completely hydrolyze to boehmite when heated in water up to 50 °C [41]; (d) H_2 molecules are released by heating RBAO powders from ~ 80 to ~ 550 °C [10, 41].

These facts suggest that such a mechanism can also apply to RBAO powders. The gaseous H_2 molecules evolved during reactions between aluminum and water (Eq. 5) or aluminum and boehmite (Eq. 7) could also originate bubbles in the RBAO-loaded, paraffin-based suspensions. During the lamination procedure at 115 °C, the reaction between aluminum and the mobile OH^- ions from its hydroxide layer produces alumina and liberates H_2 that remains entrapped at the aluminum-alumina interface. When the coalesced H_2 bubbles rupture the hydroxide layer, the newly-exposed aluminum surfaces react with the water desorbed from the surface of the RBAO powder. Thereby, more H_2 molecules are formed, according to the reaction described in (4. Then, these molecules remain entrapped in the paraffin-based suspension, remaining as voids in the sintered samples.

Therefore, the formation of bubbles in paraffin-based suspensions prepared with as-milled RBAO powders

seems to be a result of two combined effects: (i) the evaporation of physically adsorbed water from the RBAO powder surfaces and (ii) the release of H_2 from aluminum-boehmite and/or aluminum-water reactions. While the contribution of physically adsorbed water to the bubble formation can be mitigated by drying the powder at 300 °C, this temperature does not suffice to completely decompose the boehmite [10]. Therefore, the reaction between aluminum and OH⁻ ions from its hydrated surface layers can still occur in the dried powders, leading to the formation of gas bubbles in the suspension. Nevertheless, the amount and size of these bubbles are much smaller than those of samples produced with as-milled RBAO powders (see Fig. 7). Hence, drying the RBAO precursor powder at 300 °C is considered here the most appropriate solution to avoid the excessive formation of voids in the IT matrix of the fiber-reinforced RBAO-matrix composites. This procedure was therefore adopted in the manufacture of the composite $RB_{(300)}CMC$, the microstructure of which is shown in Fig. 9.

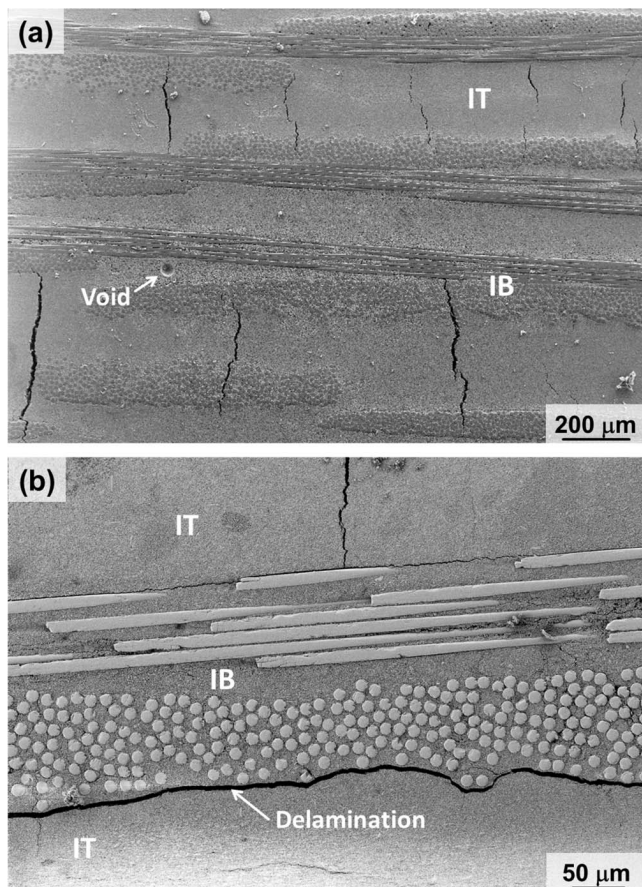**Fig. 9:** Microstructure of the composite $RB_{(300)}CMC$, produced with RBAO powders dried at 300 °C for 5 h. Sintering was performed at 1200 °C for 30 min. (a) shows the presence of a few voids and matrix cracks. Delamination along the IB and IT interfaces are indicated in (b).

Only a few voids were detected in $RB_{(300)}CMC$, as indicated in Fig. 9 (a). Nevertheless, the shrinkage-related cracks typical for 2D all-oxide CMCs were observed. This can be attributed to the partial conversion of aluminum particles to boehmite and alumina during drying at 300 °C, which reduces the amount of metallic aluminum available in the RBAO precursor powder for the compensation of

sintering shrinkage. Therefore, the compositional tailoring presented in Section II(2) should be repeated in order to select new low-to-zero shrinkage compositions for the RBAO powders dried at 300 °C.

Additionally, the use of RBAO powders dried at 300 °C changed the rheology of the paraffin-based suspension and the production of thin prepregs was no longer possible. It seems that the viscosity of the paraffin-based suspension increased, which made the lamination procedure more difficult. This resulted in a composite with thicker IT matrix layers and, consequently, with a lower fiber volume content (~21 vol%) in comparison to the $RB_{(RT)}CMC$ sample. Moreover, delamination between the IB and IT matrices was observed in some regions of the sample, as indicated in Fig. 9 (b). This suggests poor adhesion between the two composite matrices during processing. The reason for this change in the rheology of the paraffin-based suspension still needs to be investigated in future works, if RBAO matrix composites with a reduced amount of matrix defects are to be produced.

(3) Flexural properties

Table 2 summarizes the properties measured on both RBAO-matrix composites analyzed in this work. Composite $RB_{(RT)}CMC$ exhibits higher flexural strength and modulus than composite $RB_{(300)}CMC$. This is attributed to the lower fiber volume content of the latter. Representative stress-strain curves obtained by 4-point bending are presented in Fig. 10. Both composite samples present a stepped stress-strain curve, comparable to those of layered ceramics with weak interfaces [42]. This indicates a high capacity of these materials to tolerate damage, avoiding catastrophic failure. Such mechanical behavior under 4PB is typical for composites manufactured with the lamination route used in this work, as discussed in more detail elsewhere [15].

Table 2: Properties of the RBAO-matrix composites produced in this work.

Composite	$RB_{(RT)}CMC$	$RB_{(300)}CMC$
Fiber volume fraction (vol%)	36	21
Density (g/cm³)	2.55 ± 0.09	2.74 ± 0.05
Flexural strength (MPa)	243 ± 24	154 ± 16
Flexural modulus (GPa)	80 ± 5	57 ± 3
Strain at fracture (%)	0.34 ± 0.04	0.37 ± 0.09

Fig. 11 shows the fracture surface of representative 4PB samples of both RBAO-matrix composites analyzed in this work. Failure was accompanied by several interfacial delamination events in multiple layers, mainly at the interfaces between the fiber fabrics and the IB matrix. As discussed in a previous work [15], this layer-by-layer fracture leads to the stepped stress-strain curves presented in Fig. 10. After testing, all broken samples remained held together, evidencing the non-catastrophic failure. In case of composite $RB_{(300)}CMC$, failure was concen-

trated in the tensile zone of the specimens, while sample RB(RT)CMC presented bundle buckling in the compressive zone. The latter may be an effect of the presence of matrix voids in sample RB(RT)CMC, whose detrimental effects are usually more pronounced in matrix-dominated properties such as interlaminar shear strength and compressive strength [25, 26]. The influence of matrix voids on the mechanical properties of RBAO-matrix CMCs must still be investigated in more detail. Short-beam shear experiments focusing on interlaminar shear strength could, for instance, elucidate the effects of inter-textile matrix flaws on the mechanical properties of the RBAO-matrix composites.
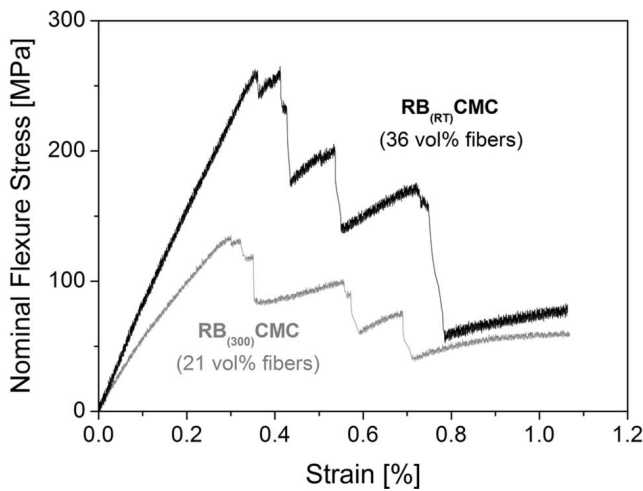

Fig. 10: Stress-strain curves of RBAO-matrix composites tested at room temperature by means of 4-point bending.
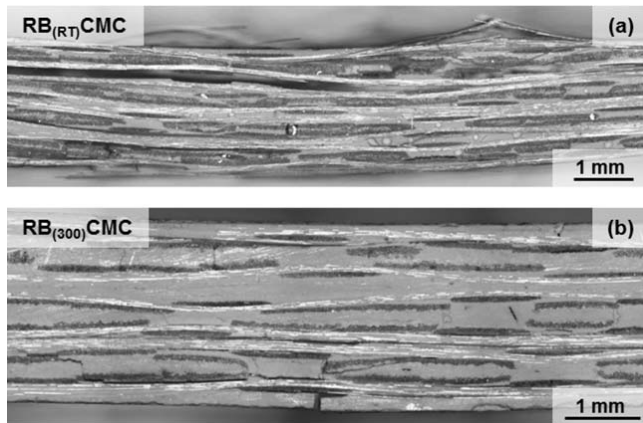

Fig. 11: Fracture surfaces of RBAO-matrix composites sintered at 1200 °C and tested at room temperature by means of 4-point bending.

IV. Concluding Remarks

Besides the potential for low shrinkage, which avoids the extensive formation of matrix cracks, the use of RBAO in the production of full-scale all-oxide composites reinforced with long alumina fibers exhibits several challenges:

• RBAO precursors must be intensively milled for several hours, in order to achieve small particle sizes that guarantee a successful oxidation process. The milling procedure leads, however, to the adsorption

of molecules (mainly water), which evolve as gas bubbles in the paraffin-based suspension used for prepreg manufacture, originating large voids in the inter-textile composite matrix.

• Although the shrinkage of RBAO matrices can be successfully tailored by varying the amount of aluminum in the precursor composition, RBAO powders are very sensitive to chemical variations due to reactions such as aluminum hydration or oxidation, which can occur either during a drying procedure or during long periods of powder storage. Such reactions decrease the amount of metallic aluminum available for shrinkage compensation and may lead to the formation of matrix cracks in the composites. Therefore, in order to profit from the zero-shrinkage tailorability of RBAO and produce crack-free, all-oxide composites, powder compositions may be adjusted any time the RBAO precursor powders endure some alteration.

Nevertheless, despite these challenges, the RBAO-matrix composites produced in this work exhibit flexural strength up to 240 MPa and a damage-tolerant behavior characterized by a stepwise stress reduction after the first failure of the material. These are promising results and should drive the further development of such composites towards the production of defect-free, all-oxide composites that can be sintered even at temperatures higher than 1200 °C.

References

1   Chawla, K.K.: Ceramic Matrix Composites, 2nd edition. Kluwer Academic Publishers, Boston, 2003.

2   Schmücker, M., Mechnich, P.: All-oxide ceramic matrix composites with porous matrices, In: Ceramic Matrix Composites. WILEY-VCH Verlag GmbH & Co., Weinheim, 2008, pp. 205 – 229.

3   Simon, R.A.: Progress in processing and performance of porous-matrix oxide/oxide composites, *Int. J. Appl. Ceram. Tec.*, **2**, [2], 141 – 149, (2005).

4   Rüdinger, A., Pritzkow, W.: The development of oxide ceramic fiber composites at the Fraunhofer ISC/HTL centre in cooperation with W.E.C. Pritzkow Spezialkeramik, (in German), *Keramische Zeitschrift*, **03**, 166 – 169, (2013).

5   Mattoni, M.A., Yang, J.Y., Levi, C.G., Zok, F.W.: Effects of matrix porosity on the mechanical properties of a porous-matrix, all-oxide ceramic composite, *J. Am. Ceram. Soc.*, **84**, [11], 2594 – 2602, (2001).

6   Mah, T., Keller, K.A., Cinibulk, M.K.: Method of making crack-free ceramic matrix composites, US 8,562,901 B1 (24 August 2009).

7   Dryden, J., Zok, F.W.: Thermal resistance of bridged cracks in fiber-reinforced ceramic composites, *J. Appl. Phys.*, **89**, [8], 4599 – 4611, (2001).

8   McDonald, K.R., Dryden, J.R., Zok, F.W.: Effects of matrix cracks on the thermal diffusivity of a fiber-reinforced ceramic composite, *J. Am. Ceram. Soc.*, **84**, [9], 2015–2021, (2001).

9   Claussen, N., Le, T., Wu, S.: Low-shrinkage reaction-bonded alumina, *J. Eur. Ceram. Soc.*, **5**, 29–35, (1989).

10   Holz, D., Wu, S., Scheppokat, S., Claussen, N.: Effect of processing parameters on phase and microstructure evolution in RBAO ceramics, *J. Am. Ceram. Soc.*, **77**, [10], 2509–2517, (1994).

11   Janssen, R., Wendorff, J., Claussen, N.: Fiber reinforcement of reaction bonded oxide ceramics, In: High-Temperature Ceramic-Matrix Composites II. The American Ceramic Society, Westerville, 1995, pp. 167–173.

12   Keller, K.A., Mah, T., Boakye, E.E., Parthasarathy, T.A.: Gelcasting and reaction bonding of oxide-oxide minicomposites with monazite interphase, **21**, [3], 525–534, (2000).

13   Wendorff, J.: Synthesis and properties of long-fibre-reinforced oxide ceramic composites for high-temperature applications, (in German),VDI Verlag GmbH, Düsseldorf, 1997.

14   Guglielmi, P.O., Blaese, D., Hablitzel, M.P., Nunes, G.F., Lauth, V.R., Garcia, D., Al-Qureshi, H.A., Hotza, D., Janssen, R.: Multilayered fiber-reinforced oxide composites produced by lamination of thermoplastic prepregs, *Adv. Sci. Technol.*, **89**, 145–150, (2014).

15   Guglielmi, P.O., Blaese, D., Hablitzel, M.P., Nunes, G.F., Lauth, V.R., Hotza, D., Al-Qureshi, H.A., Janssen, R.: Microstructure and flexural properties of multilayered fiber-reinforced oxide composites fabricated by a novel lamination route, *Ceram. Int.*, (2015).

16   Claussen, N., Janssen, R., Holz, D.: Reaction bonding of aluminum oxide (RBAO), *J. Ceram. Soc. Jpn.*, **103**, [8], (1995).

17   Wu, S., Claussen, N.: Reaction-bonding of ZrO_2-containing Al_2O_3, *Solid State Phenom.*, **25–26**, 293–300, (1992).

18   Sheedy, P.M., Caram, H.S., Chan, H.M., Harmer, M.P.: Effects of zirconium oxide on the reaction bonding of aluminum oxide, *J. Am. Ceram. Soc.*, **84**, [5], 986–990, (2001).

19   Goushegir, S.M., Guglielmi, P.O., da Silva, J.G.P., Hablitzel, M.P., Hotza, D., Al-Qureshi, H.A., Janssen, R.: Fiber-matrix compatibility in an all-oxide ceramic composite with RBAO Matrix, *J. Am. Ceram. Soc.*, **95**, [1], 159–164, (2012).

20   Coronel, J.J., Janssen, R., Claussen, N.: Shaping of ceramic parts from powder-loaded wax suspensions, (in Spanish), *Bol. Soc. Esp. de Ceram.*, **48**, [5], 843–848, (2004).

21   Leverköhne, M., Coronel, J., Hupert, D., Gorlov, I., Janssen, R., Claussen, N.: Novel binder system based on paraffin-wax for low-pressure injection molding of metal-ceramic powder mixtures, *Adv. Eng. Mater.*, **3**, [12], 995–998, (2001).

22   DIN Deutsches Institut für Normung e.V.: Mechanical properties of ceramic composites at room temperature - Part 3: Determination of flexural strength **81.060.30** (DIN EN 658–3:2002–11) (Beuth Verlag GmbH, Berlin, 2002).

23   ASTM International: Standard test method for flexural properties of continuous fiber-reinforced advanced ceramic composites (C 1341–00) (ASTM, 2000).

24   Varna, J., Joffe, R., Berglund, L.A., Lundström, T.S.: Effect of voids on failure mechanisms in RTM laminates, *Compos. Sci. Technol.*, **53**, 241–249, (1995).

25   Jeong, H.: Effects of voids on the mechanical strength and ultrasonic attenuation of laminated composites, *J. Compos. Mater.*, **31**, [3], 276–292, (1997).

26   Costa, M.L., de Almeide, S.F.M., Rezende, M.C.: The influence of porosity on the interlaminar shear strength of carbon/epoxy and carbon/bismaleimide fabric laminates, *Compos. Sci. Technol.*, **61**, 2101–2108, (2001).

27   Hagstrand, P.-O., Bonjour, F., Manson, J.-A.E.: The influence of void content on the structural flexural performance of unidirectional glass fiber reinforced polypropylene composites, *Composites Part A*, **36**, 705–714, (2005).

28   Janssen, R., Claussen, N., Scheppokat, S., Roeger, M.: Reaction bonding and reactive sintering: a way to low cost manufacturing of alumina based components, *Materials Integration*, **15**, [4], 75–79, (2002).

29   Temuujin, J., Coronel, J.J., Minjigmaa, A., Mackenzie, K.: Water content and water evolution from reaction-bonded aluminum oxide (RBAO) powder precursors, *Int. J. Appl. Ceram. Techn.*, **5**, [3], 289–294, (2008).

30   Wu, S., Holz, D., Claussen, N.: Mechanisms and kinetics of reaction-bonded aluminum oxide ceramics, *J. Am. Ceram. Soc.*, **76**, [4], 970–980, (1993).

31   Watson, M.J., Chan, H.M., Harmer, M.P., Caram, H.S.: Effects of milling liquid on the reaction-bonded aluminum oxide process, *J. Am. Ceram. Soc.*, **81**, [8], 2053–2060, (1998).

32   Gitzen, W.H.: Alumina as a ceramic material, the american ceramic society inc., Columbus, Ohio, 1970.

33   Sato, T.: Thermal decompostion of aluminium hydroxides, *J. Therm. Anal.*, **32**, 61–70, (1987).

34   Deng, Z.-Y., Ferreira, J.M.F., Tanaka, Y., Ye, J.: Physicochemical mechanism for the continuous reaction of gamma-Al_2O_3-modified aluminum powder with water, *J. Am. Ceram. Soc.*, **90**, [5], 1521–1526, (2007).

35   Guglielmi, P.O., Silva, W.R.L., Repette, W.L., Hotza, D.: Porosity and mechanical strength of an autoclaved clayey cellular concrete, *Advances in Civil Engineering*, **2010**, 1–6, (2010).

36   Scheffler, Colombo, P., eds.: Cellular ceramics. structure, manufacturing, properties and applications, WILEY-VCH Verlag GmbH & Co., Weinheim, 2005.

37   Chaklader, A.C.D.: Hydrogen generation from water split reaction, US 6440385 B1 (14 August 2000).

38   Deng, Z.-Y., Liu, Y.-F., Tanaka, Y., Ye, J., Sakka, Y.: Modification of Al particle surfaces by gamma-Al_2O_3 and its effect on the corrosion behavior of Al, *J. Am. Ceram. Soc.*, **88**, [4], 977–979, (2005).

39   Petrovic, J., Thomas, G.: Reaction of aluminum with water to produce hydrogen. *A study of issues related to the use of aluminum for on-board vehicular hydrogen storage*, (2008).

40   Bunker, B.C., Nelson, G.C., Zavadil, K.R., Barbour, J.C., Wall, F.D., Sillivan, J.P.: Hydration of passive oxide films on aluminum, *J. Phys. Chem. B*, **106**, (18), 4705–4713, (2002).

41   Holz, D.: Production and characterization of reaction-bonded Al_2O_3 ceramics (RBAO process) based on the example of the Al_2O_3/ZrO_2 system, (in German), VDI-Verlag GmbH, Düsseldorf, 1994.

42   Clegg, W.J., Kendall, K., Alford, N.M., Button, T.W., Brichall, J.D.: A simple way to make tough ceramics, *Nature*, **347**, 455–457, (1990).